Eng. Sci., 2025, **37**, 1813

Engineered Science
DOI: https://dx.doi.org/10.30919/es1813

# Mechanically Robust Continuous Fiber-Reinforced Composites with Synergistic Light/Electric Responsiveness and Wireless Internet of Things-Enabled Actuation

Lin Jiang,[1,2,*] Xingyu Yue,[1] Jie Sheng,[1] Mingxia Li,[1] Shengkun Jiang,[1] Zhengqiang Huang,[3] Tie Geng[1] and Haihong Wu[1]

## Abstract

Stimulus-responsive bilayer actuators play a vital role in next-generation intelligent systems. However, their practical applications are often hindered by limited mechanical robustness, weak interfacial adhesion, and complex fabrication processes. Herein, a scalable bilayer actuator is developed via thermal pressing of a polylactic acid (PLA) layer with continuous carbon fibers (CFs) reinforcement. The mismatch in thermal expansion coefficients between the active PLA and passive CFs layers enables programmable and complex deformation under external stimuli. The incorporation of continuous CFs endows the actuator with enhanced mechanical performance (tensile strength: 1525 MPa), while the interfacial bonding strength reaches 335 N/m, ensuring structural integrity over 500 actuation cycles. The actuator exhibits light-induced bending of 142° within 14 s under 0.9 W/cm2 illumination, and electrothermal actuation of 160° at 2.3 V. Notably, a synergistic actuation effect is observed under combined light and electrical stimulation, revealing a coupled mechanism that expands current understanding of multi-stimuli actuation. An internet of things (IoT)-enabled wireless control system is further integrated, enabling real-time manipulation of a deployable foldable structure, which could be applied to solar sail protection on space stations. This work presents a high-performance actuator platform that combines mechanical robustness, multi-responsiveness, and intelligent control, offering broad potential for applications in adaptive structural systems.

*Keywords:* Bilayer actuator; Continuous carbon fiber-reinforced composites; Stimulus responsiveness; Synergistic actuation; Wireless foldable structure.
Received: 28 July 2025; Revised: 22 September 2025; Accepted: 10 October 2025.
Article type: Research article.

## 1. Introduction

Continuous fiber-reinforced composites (CFRCs) have been widely employed in aerospace, automotive, civil infrastructure, and emerging intelligent systems due to their exceptional mechanical properties, low density, and outstanding designability.[1-3] Especially, continuous carbon fibers (CFs)-based composites exhibit high tensile strength, dimensional stability, and tailorable anisotropy, making them highly suitable for load-bearing structures in harsh or dynamic environments.[4-7] However, most existing CFRCs are structurally passive—they serve as mechanically robust carriers but lack the capacity to actively respond to external stimuli such as light, electricity, or heat. The absence of stimulus-responsiveness severely limits their functionality in future intelligent and adaptive structural systems.[8] Therefore, enabling actuation or adaptive deformation functions in CFRCs without compromising their inherent strength is of great scientific and technological importance.

Among current strategies for designing stimulus-responsive actuators, bilayer architectures have gained significant attention due to their simple structure and controllable deformation mechanisms.[9,10] These actuators typically consist of two layers with contrasting thermal expansion coefficients (CTEs), where external stimuli, inculding thermal, photothermal, or electrothermal, induce

[1] *Henan International Joint Laboratory of Carbon Fiber Composite Material, School of Mechanical and Electrical Engineering, Henan University of Technology, Zhengzhou, 450001, China*
[2] *School of Mechanical and Electrical Engineering, Zhengzhou University of Industrial Technology, Zhengzhou, 450001, China*
[3] *Zhong Yuan Institute, Zhejiang University, Zhengzhou, 450001, China*
**E-mail:* jianglin@haut.edu.cn (J. Lin)

interfacial strain mismatch and subsequent bending deformation.[11,12] Such bilayer configurations provide a straightforward method to engineer programmable shape morphing behaviors and have been extensively applied in shape-changing soft robots and adaptive interfaces.[13,14]

Continuous CFs present unique advantages when introduced into bilayer actuator designs. First, they possess an almost zero or even negative CTE along the fiber direction, providing strong passive resistance to thermal expansion and enabling efficient bending when paired with a thermally expandable layer such as polylactic acid (PLA).[15,16] Second, CFs inherently exhibit photothermal and electrothermal conversion abilities due to their excellent electrical and optical absorption characteristics,[17,18] making multi-mode stimulus responses feasible within a single material system. Third, the in-plane anisotropy of unidirectional CFs provides additional freedom for deformation pattern design and programmable actuation, allowing for complex, directional, or asymmetric shape changes.[19] Most importantly, the incorporation of continuous CFs significantly enhances the mechanical performance of actuators, enabling their potential deployment in load-bearing intelligent structures.[20] Despite these advantages, the use of continuous fibers in responsive actuators has been scarcely reported, and their integration remains technically challenging. Further research is needed to explore their applicability and enable their effective use in smart actuator platforms.

Furthermore, existing studies on stimulus-responsive actuators largely focus on single-mode actuation, particularly light-induced or electrically driven deformation.[21,22] However, light and electrical stimuli are inherently limited in actuation depth, intensity, and controllability when applied independently. In contrast, synergistic actuation using combined light and electrical stimulation holds promise to overcome these limitations.[23,24] By leveraging multi-stimulus coupling, the required intensity of each individual input can be reduced while achieving enhanced or programmable deformation.[25-27] Despite its significance, the understanding of coupled light/electric actuation mechanisms remains limited, with few systematic investigations available in current literature. Addressing this knowledge gap would provide valuable insight for designing more efficient, low-power, and multifunctional actuator systems.

Here, we report a scalable bilayer actuator fabricated by thermally pressing a PLA layer with a continuous carbon fiber layer, forming a heterogeneous and asymmetric structure. Through optimized thermal pressing parameters and fiber orientation, we achieve tunable bending behaviors based on CTE mismatch. We further utilize the anisotropy of CFs to program complex deformation modes. Systematic investigations are conducted on the thermal, light-induced, electrically induced, and light/electric synergistic actuation behaviors, and the underlying coupling mechanisms are analyzed in detail. Finally, to demonstrate application feasibility, we integrate an internet of things (IoT)-enabled wireless control system, enabling real-time actuation of a foldable deployable structure. This work not only advances the understanding of synergistic stimulus-responsive mechanisms in continuous fiber composites, but also provides a practical and scalable platform for the development of robust, programmable, and intelligent actuator systems.

## 2. Experimental

### 2.1 Materials

Polylactic acid pellets (PLA, 2002D, density: 1.20–1.30 g/cm³) were purchased from NatureWorks, USA. The carbon fiber prepreg sheets (thickness: 0.08 mm), containing T700 CFs (diameter: 7–8 μm) and an epoxy-amine resin matrix, were obtained from Weihai Guangwei Composites Co., Ltd., China. Dichloromethane (DCM, AR grade, boiling point: 39.8 °C) was supplied by Chengdu Cologne Chemicals Co., Ltd., China. All materials were used as received without further purification.

### 2.2 Fabrication of CF/PLA composite actuator

#### 2.2.1 Preparation of PLA film

PLA films were fabricated via a spin-coating method. Briefly, PLA pellets were dissolved in DCM to form a 14 wt.% solution, stirred at room temperature until fully homogeneous, and then degassed for 3 min to eliminate air bubbles. The resulting solution was spin-coated onto a glass substrate at 1500 rpm for 30 s, followed by drying at 40 °C to remove the solvent, yielding uniform PLA films with a thickness of 50 ± 2 μm.

#### 2.2.2 Preparation of bilayer CF/PLA composites

Bilayer CF/PLA composites were fabricated via thermal pressing. A layer of CF prepreg was first laid on the mold surface, followed by the PLA film. After precise alignment, the stacked layers were placed into the preheated mold cavity and hot-pressed at 4 MPa for 20 min under various temperatures (130 °C, 150 °C, 170 °C, and 190 °C). The samples were demolded after cooling and labeled as TCF-1, TCF-2, TCF-3, and TCF-4, respectively.

### 2.3 Characterization

#### 2.3.1 Morphology and structure characterization

The microstructure of CF/PLA actuators was examined using

scanning electron microscopy (SEM, SU8010, Hitachi, Japan). Prior to imaging, samples were sputter-coated with a ~10 nm gold layer. SEM images were acquired at an accelerating voltage of 10 kV.

#### 2.3.2 Mechanical testing

Tensile properties were evaluated using a universal testing machine (UTM 5105, China). CF/PLA specimens were prepared with fiber orientations of 0°, 30°, 45°, 60° and 90°, with dimensions of 250 mm × 25 mm. Tests were conducted at room temperature (23 ± 2 °C) with a crosshead speed of 1 mm/min. Five specimens were tested for each group, and average values with standard deviations were reported.

#### 2.3.3 Interfacial peeling test

The interfacial adhesion strength between the CF and PLA layers was characterized using a T-peel test.[28] To create a localized interfacial separation zone, a polyimide film was inserted between the CF prepreg and PLA film prior to thermal pressing, covering approximately half of the contact area. After curing, the polyimide film was peeled off to generate a controlled delamination region. The two free ends of the CF and PLA layers were then clamped in a universal testing machine, and the test was performed at a constant speed of 1 mm/min.

#### 2.3.4 Thermal-response behavior

The thermal actuation behavior of the CF/PLA bilayer actuator was investigated using a precision temperature-controlled heating stage (SET, Shenzhen Fanyuhang Electronics Co., Ltd., China). Rectangular specimens (20 mm × 25 mm × 0.1 mm) were tested at various temperatures (80 ℃, 100 ℃, 120 ℃, 140 ℃, and 160 ℃) to evaluate their deformation response. To examine the effect of carbon fiber anisotropy on actuator deformation, bilayer samples with different fiber orientations (0° to 180°, at 15° intervals) were prepared, all with dimensions of 10 mm × 50 mm. The dynamic deformation process was recorded in real time using a high-resolution camera (iPhone, 4K/60 fps, USA), and key deformation parameters were extracted and analyzed using digital image correlation techniques with image processing software (Camera Measure Pro V2.3, China).

#### 2.3.5 Light-response behavior

To evaluate the light-stimulated actuation behavior of the CF/PLA actuator, an infrared heating lamp (Philips IR375R, 100-375 W, wavelength: 570-600 nm) was used to adjust the light intensity in the range of 0.3-1.2 W/cm². Samples with dimensions of 20 mm × 25 mm were tested. During actuation, the surface temperature of the actuator was monitored in real time using an infrared thermal imaging camera (Testo865, Testo, Germany).

#### 2.3.6 Electric-response behavior

Electrical actuation was investigated using a programmable DC power supply (Maisheng MS-1520DS, China) with applied voltages ranging from 0.3 to 2.3 V. Specimens (35 mm × 50 mm) were connected via conductive copper tape electrodes. Temperature evolution during actuation was monitored using the Testo 865 thermal imaging system.

#### 2.3.7 Light and electric synergistic response behavior

To investigate the synergistic actuation behavior under combined light and electrical stimuli, a dual-mode stimulation system was constructed, consisting of an infrared lamp (Philips IR375R) and a programmable direct current (DC) power supply (Maisheng MS-1520DS). CF/PLA actuators (35 mm × 50 mm) were subjected to simultaneous light irradiation (0-1.0 W/cm²) and electrical input (0-2.4 V). Real-time surface temperature fields were recorded using the Testo 865 thermal imaging system.

## 3. Results and discussion

### 3.1 Structural design and actuation mechanism of the actuator

Heterogeneous bilayer structures represent a key configuration in the design of intelligent actuators. Typically, such systems consist of a thermally responsive active layer and a dimensionally stable passive layer, where the mismatch in their thermal expansion coefficients drives the overall deformation.[11,29,30] The rational selection of material systems and structural design is crucial for achieving high-performance actuators capable of responding to multiple external stimuli. Continuous CFs, with their high specific strength, anisotropic mechanical properties, and near-zero or even negative CTE,[31] as well as excellent photothermal and electrothermal conversion capabilities, are ideal candidates for the passive layer. In contrast, thermoplastic polymers such as polylactic acid (PLA) possess relatively high CTEs and favorable thermal processability, making them suitable as active layers.[32,33] Integrating CF and PLA into a heterogeneous bilayer configuration holds promise for realizing actuators that combine excellent mechanical robustness with efficient responsiveness under thermal, light, and electrical stimuli.

To validate this design concept, a spin-coating and hot-pressing strategy was employed to fabricate PLA/CF bilayer actuators (Fig. 1a). Uniform, stress-free PLA films were first

prepared via spin-coating to ensure continuity and flexibility of the active layer during actuation. These films were then uniformly placed over pre-laid continuous CF prepregs to establish intimate interfacial contact prior to thermal pressing. By optimizing the processing parameters, strong interfacial bonding between the PLA and CF layers was achieved, while preserving the structural integrity of the PLA layer and preventing its penetration into the fiber network. This ensured the structural heterogeneity necessary for effective bilayer actuation.

As illustrated in Fig. 1(b), the resulting heterogeneous bilayer composite undergoes actuation upon exposure to thermal, light, or electrical stimuli. The CF layer exhibits negligible volume change, whereas the PLA layer undergoes significant expansion or contraction, providing the primary driving force for bending deformation. This actuator is fabricated using only widely available thermoplastic films and commercial CF prepregs, avoiding the need for expensive nanomaterials or complex synthesis processes. As such, it offers significant cost advantages and excellent scalability for practical engineering applications. Furthermore, the scalable hot-pressing process enables efficient integration of materials with distinct thermal expansion properties, accelerating actuation response. The high anisotropy of CFs not only contributes to mechanical stiffness but also constrains and guides the deformation of the surrounding polymer matrix, enabling programmable and complex actuation modes. In summary, this actuator demonstrates promising potential with excellent mechanical properties and multi-stimuli responsiveness.

### 3.2 Process optimization of the heterogeneous bilayer structure

To construct CF/PLA bilayer composites with pronounced structural heterogeneity, the hot-pressing temperatures were selected based on the thermal stability of continuous carbon fiber (CF) prepregs and the thermal transitions of PLA.[34,35] The selected temperature range (130 °C, 150 °C, 170 °C, and 190 °C) spans the critical phase transition region of PLA from glass transition to complete melting. Fig. 2(a) shows the cross-sectional structures of the CF/PLA composites prepared at different temperatures. The results indicate that the thickness of the CF layer remains nearly constant (~0.08 mm) across all temperatures, whereas the PLA layer becomes progressively thinner with increasing temperature, leading to a gradual reduction in heterogeneity. At 190 °C, the low-viscosity PLA visibly infiltrates the CF layer, resulting in a nearly homogeneous structure. At 130 °C, the actuator formed a complete PLA layer (~0.04 mm thick). SEM images of the cross-section of the CF in both 0° and 90° orientations (Fig. S1) clearly show a stable bilayer morphology. This indicates that the process preserves the integrity of the PLA layer and promotes the formation of a heterogeneous structure between the PLA matrix and the CF layer.

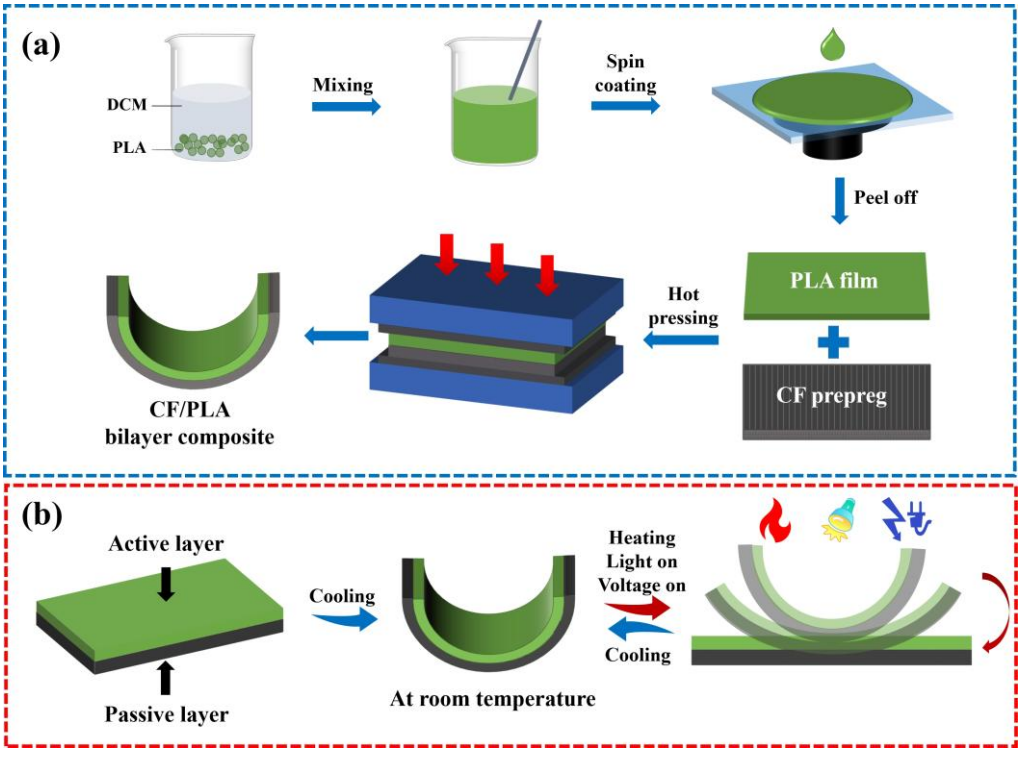


**Fig. 1:** Schematic illustration of (a) the fabrication process and (b) the actuation mechanism of the CF/PLA bilayer actuator.

As shown in Fig. 2(b), actuators with greater heterogeneity display more pronounced initial curvature. Finite element simulations (Fig. 2c) further confirm this trend, indicating that higher heterogeneity leads to greater residual stress accumulation at the interface. This enhances internal energy storage and drives spontaneous curvature formation in the absence of external forces.[36] The degree of curvature was quantitatively evaluated using the three-point arc fitting method, as illustrated in Fig. 2(d). By connecting the arc endpoints A and C with the midpoint B and constructing perpendicular bisectors, their intersection point O defines the radius R of curvature, and the curvature is calculated as 1/R. Quantitative results of initial curvature for samples formed at different temperatures are shown in Fig. 2(e). The sample fabricated at 130 ℃ (TCF-1) exhibits the highest curvature of 0.196 $mm^{-1}$, which gradually decreases with increasing temperature, reaching a minimum of only 0.037 $mm^{-1}$ at 190 ℃.

In summary, thermal pressing at 130 °C effectively maintains interfacial integrity and structural heterogeneity between CF and PLA layers, yielding the largest initial deformation. Therefore, 130 °C was selected as the optimal fabrication temperature for the bilayer actuator. All actuator samples discussed in the following sections were prepared under this condition.

### 3.3 Physicochemical properties and thermally induced actuation behavior

Due to the inherent anisotropy of CFs, the CF/PLA bilayer actuator exhibits pronounced direction-dependent mechanical properties. As shown in Fig. 3(a), tensile tests were performed on samples with fiber orientations of 0° and 90°. The actuator with fibers oriented at 90° (perpendicular to the loading direction) exhibited a tensile strength of 46 MPa, whereas the 0° sample (parallel to the fiber direction) achieved a significantly higher strength of 1525 MPa, benefiting from the reinforcement of continuous CFs. This superior mechanical strength surpasses that of most reported soft actuators,[7,37,38] highlighting its potential for deployment in complex environments. To further evaluate the interfacial bonding strength, T-peel tests were conducted (Fig. 3b). The measured peel strength reached 335 N/m, confirming the formation of a

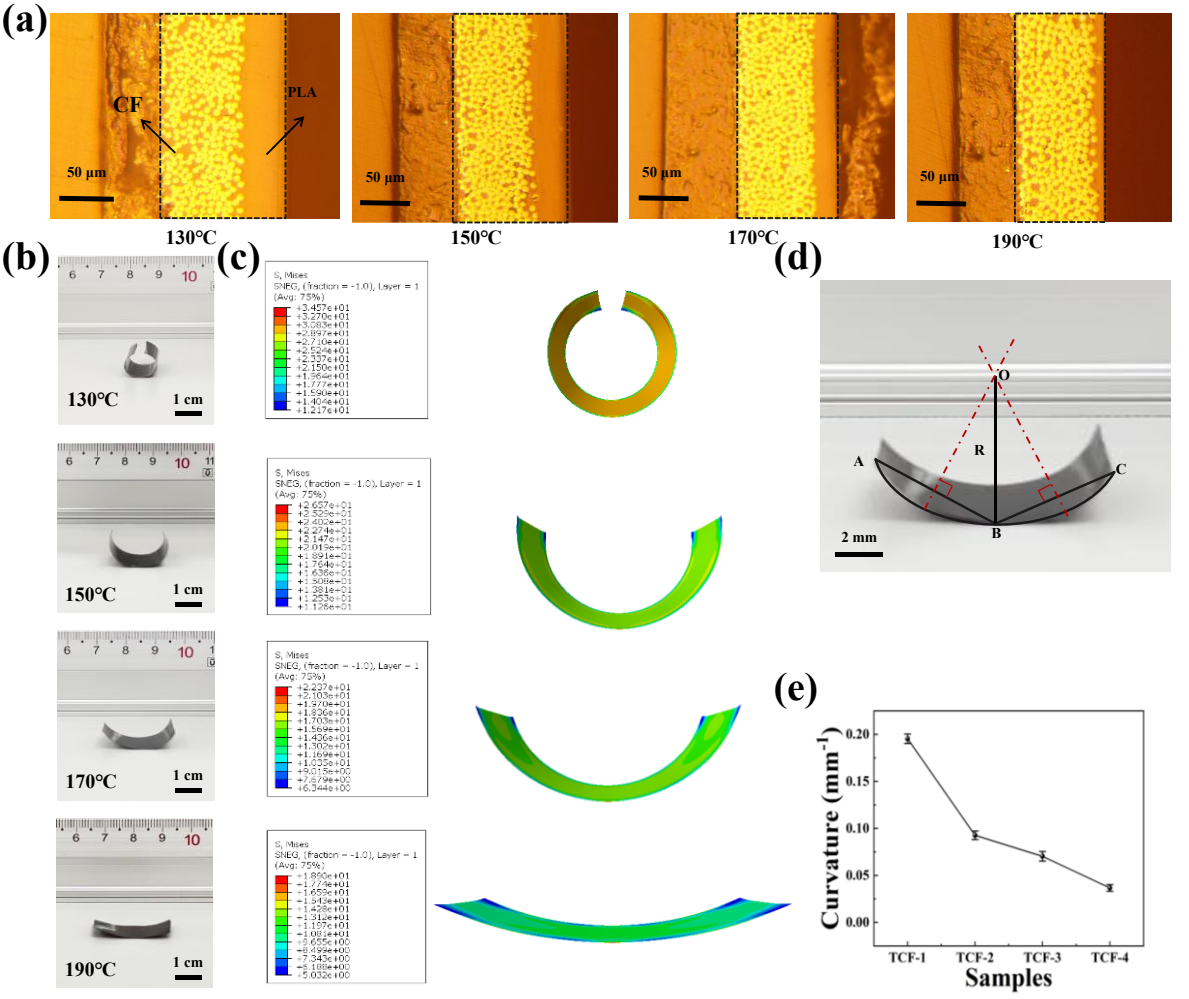


**Fig. 2:** Characterization of CF/PLA actuators fabricated at different hot-pressing temperatures: (a) Cross-sectional optical images; (b) Photographs of initial actuator shapes; (c) Finite element simulation of stress distribution; (d) Schematic illustration of curvature calculation using the three-point arc fitting method; (e) Initial curvature values of the actuators.

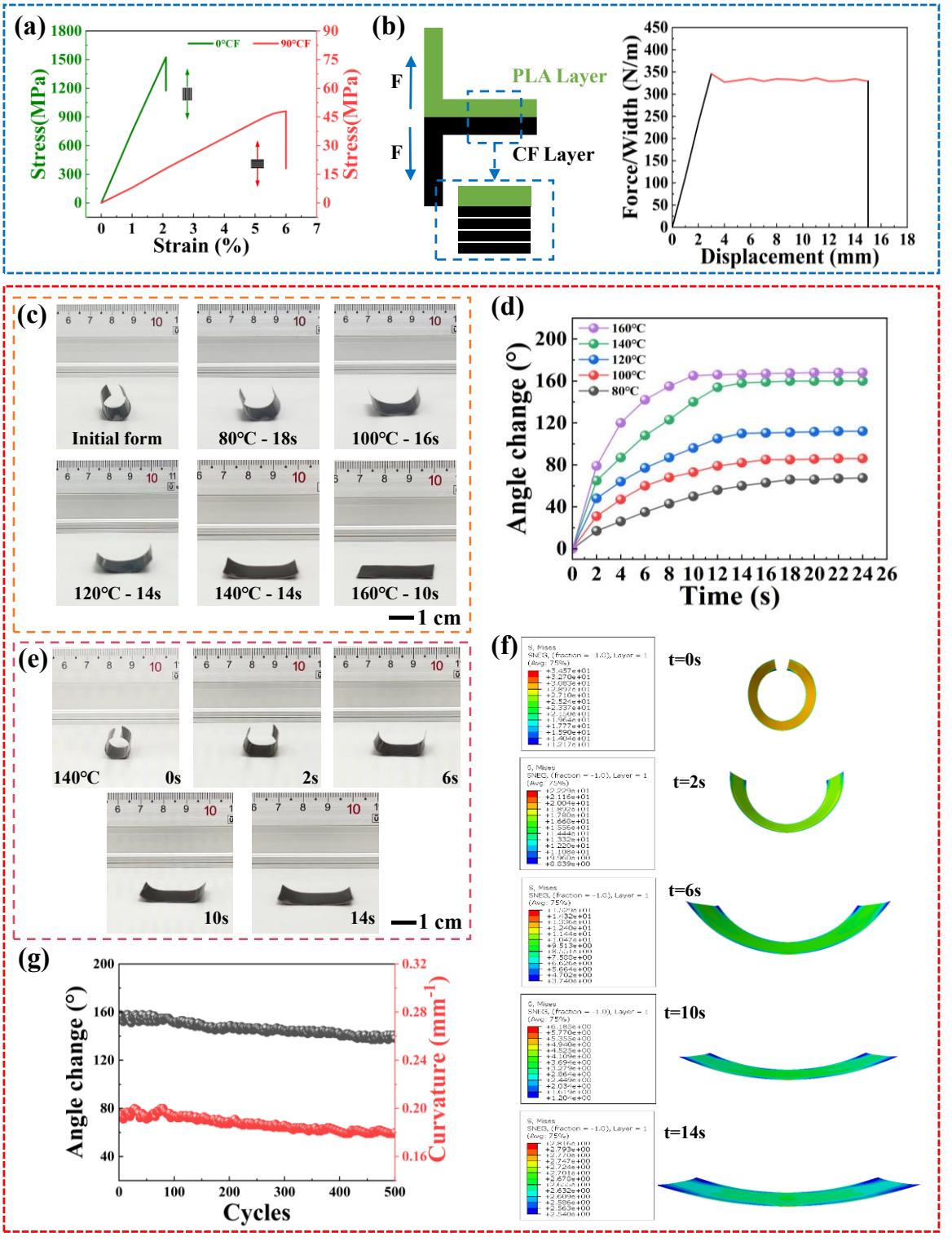


**Fig. 3:** Mechanical and actuation behavior of CF/PLA bilayer actuators: (a) Tensile stress-strain curves with 0° and 90° fiber orientations; (b) Schematic diagram of the interfacial peeling test and corresponding peel strength results; (c) Optical images of actuators at equilibrium states under different actuation temperatures; (d) Time-dependent bending angles under thermal stimuli; (e) Time-resolved actuation behavior under 140 °C; (f) Finite element simulation of stress evolution in the actuator during thermal actuation at 140 °C; (g) Bending stability and shape retention of the actuator over 500 thermal actuation cycles at 140 °C.

robust interface between the CF and PLA layers, and validating the feasibility and reliability of the hot-pressing process in constructing high-performance bilayer structures.

To systematically investigate the effect of temperature on actuation behavior, thermal stimuli ranging from 80 to 160 °C were applied. Fig. 3(c) illustrates the initial morphology of the actuator, as well as the final configuration and response time under different temperatures. The angular deformation was

quantified using an image-based measurement method, the deformation angle is the difference between $\alpha_1$ and $\alpha_2$ (Fig. S2), and the results are presented in Fig. 3(d). With increasing temperature, both the deformation amplitude and response rate improved significantly. Specifically, at 80 °C, the relatively small mismatch in thermal expansion between CF and PLA resulted in limited deformation and prolonged response time. In contrast, at 160 °C, the actuator unfolded from its curled state to a nearly flat configuration within 10 s. This enhancement is primarily attributed to the intensified thermal expansion of PLA at elevated temperatures, which generates a greater internal driving force and facilitates a more rapid bending response.

To provide a representative demonstration of the actuation process, 140 °C was selected as the characteristic stimulus temperature. As shown in Fig. 3(e) and Movie S1, the actuator achieved an angular deformation exceeding 100° within the first 6 s of thermal stimulation. Subsequently, as heating continued, the molecular chains in the PLA layer approached a dynamic equilibrium, leading to partial relaxation of the thermal expansion stress and a deceleration of the deformation rate. The actuator ultimately reached a steady-state configuration after 14 s. Furthermore, finite element simulations of the internal stress distribution (Fig. 3f) revealed the evolution of interfacial stresses during actuation. At 0 s, the actuator exhibited a curled configuration, with significant stress concentrations at the interface, reaching a maximum value of 30.8 Pa. Upon heating, thermal expansion of the PLA layer progressively counteracted the initial residual stress, promoting the gradual unfolding of the bilayer structure. By 14 s, the actuator was nearly fully extended, indicating that most of the stored internal stress had been released. In addition, the CF/PLA actuator demonstrated excellent thermal actuation stability and cycling reliability. As shown in Fig. 3(g), during 500 continuous deformation cycles, the bending angle gradually decreased from 158° to 142°, with a fluctuation of only 10.7%, and the bending curvature dropped from 0.200 $mm^{-1}$ to 0.179 $mm^{-1}$, with a variation of just 11.3%, confirming its long-term durability and repeatability.

### 3.4 Complex deformation behavior of the actuator

Compared with conventional actuators limited to simple, single-mode deformation, the CF/PLA bilayer actuator exhibits the potential for complex and programmable deformation due to the anisotropic characteristics of CFs.[39-41] In this bilayer structure, the elastic modulus of CFs along the 0° direction is significantly higher than that of the PLA matrix. As a result, the deformation behavior strongly depends on fiber orientation, exhibiting directional expansion or contraction.

To systematically investigate the effect of fiber orientation on actuation morphology, a series of actuators with fiber angles of 0°, 15°, 30°, 45°, 60°, 75°, 105°, 120°, 135°, 150°, 165°, and 180° were fabricated. The fiber orientation angle is defined as the angle between the actuator's longitudinal axis and the alignment direction of CFs, with the cutting strategy shown in Fig. S3. As shown in Fig. 4(a), two types of helical deformation were observed. Specifically, when the fiber angle is within 0°-90°, the actuators form a left-handed helix; as the angle increases to 90°-180°, the structure transitions into a right-handed helix. The degree of coiling increases progressively as the fiber angle approaches 90°, and deformation behaviors in the 90°-180° range are mirror-symmetric to those in the 0°-90° range.

For a more precise analysis of fiber orientation effects on helical geometry, three geometric parameters were defined for both left- and right-handed helices, as illustrated in Fig. 4(b): axial length, pitch, and coil diameter. As shown in Fig. 4(c), the axial length and pitch decrease as the fiber angle approaches 90°, corresponding to increasingly pronounced coiling. At a 90° orientation, the axial length and pitch reach their minimum values of 9.5 mm and 0 mm, respectively, forming a tightly coiled cylindrical shape. Owing to the geometric symmetry of the 0°-90° and 90°-180° configurations, the actuators generate mirror-symmetric torsional deformations with opposite directions and comparable axial lengths. Furthermore, despite varying fiber orientations, all actuators display similar coil diameters. This is attributed to the consistent interfacial structure across samples, which results in equivalent internal stress levels and thus comparable coil diameters.

To further evaluate the mechanical robustness of these actuators, tensile tests were performed on specimens with fiber orientations of 0°, 30°, 45°, 60°, and 90°. As shown in Fig. S4, the tensile strength gradually decreases with increasing fiber orientation angle, reflecting the anisotropic mechanical behavior of fiber-reinforced composites. Nevertheless, the overall tensile performance remains superior to that of most reported soft actuators,[7,37,38] confirming the mechanical advantages of the CF/PLA system. In summary, by tailoring the orientation of continuous CFs, programmable deformation of CF/PLA actuators can be effectively achieved. This provides both theoretical support and design guidance for the development of complex motion modes in flexible devices and intelligent structures.

### 3.5 Light- and electricity-triggered actuation behavior

To evaluate the light-responsive behavior of the CF/PLA bilayer actuator, its surface temperature evolution was systematically measured under varying light intensities (0.25-1.20 $W/cm^2$), as shown in Fig. 5(a). The equilibrium temperature increased significantly with light intensity: at 0.5 $W/cm^2$, the maximum temperature reached 101 °C, while at 0.9 $W/cm^2$, it rapidly rose to 160 °C, enabling the actuator to fully unfold from its curled state. To further illustrate the photothermal conversion capability, the surface temperature evolution under continuous irradiation at 0.9 $W/cm^2$ was recorded (Fig. 5b). A sharp temperature increase was observed in the initial 12 s, reaching 141 °C, followed by a slower rise until stabilizing at 150 °C after 20 s. Infrared thermography

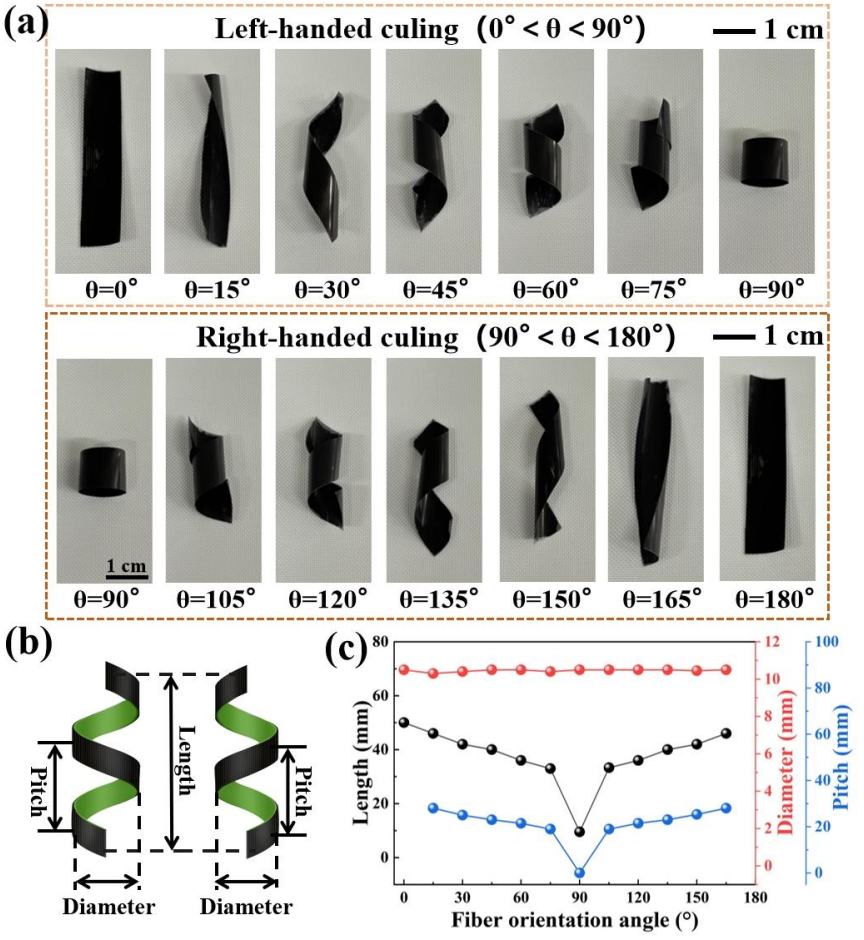


**Fig. 4:** Complex deformation behavior of the CF/PLA bilayer actuators: (a) Initial configurations of rectangular actuators with different fiber orientations; (b) Geometric models and key structural parameters (axial length, pitch, coil diameter) of left- and right-handed helices; (c) Variation of helical geometry as a function of fiber orientation angle under thermal actuation.

confirmed uniform heat distribution across the actuator surface without local hotspots. The actuation rate and deformation amplitude were also strongly dependent on light intensity (Fig. 5c). At 0.5 W/cm², the actuator achieved a bending angle of only 58° within 14 s, whereas at 0.9 W/cm², it reached 142° under the same duration. Notably, the actuator could spontaneously recover to its original curled state upon removal of the light source, demonstrating excellent reversibility and shape memory behavior.

In addition to light responsiveness, the CF/PLA actuator also exhibited electrically driven actuation, enabled by the excellent electrothermal conversion capability of continuous CFs.[42] Fig. 5(d) presents the surface temperature variation under different applied voltages. The equilibrium temperature increased nearly linearly with voltage: from 36 ℃ at 0.25 V to 170 ℃ at 2.3 V. This electrothermal response followed Joule's law ($Q = U^2t/R$), where increased voltage led to more efficient conversion of electrical energy into thermal energy, thus enabling controlled deformation of the actuator. As shown in Fig. 5(e), under a constant voltage of 2.3 V, the surface temperature rose from ambient to 150 ℃ within 20 s, and stabilized at 170 ℃ after 35 s. This excellent electrothermal response stemmed from the low electrical resistivity of the CFs (~0.3 Ω·m), which minimized energy loss and enhanced energy conversion efficiency. Long-term reliability was evaluated under continuous heating at 2.2 V (Fig. 5f), showing minimal temperature fluctuation (<±1.5%), confirming stable and repeatable actuation performance.

The results of both light- and electrically triggered actuation fully demonstrate the application potential of the CF/PLA bilayer actuator in intelligent actuation and flexible electronics. To further visualize its practical response, a locally irradiated actuator with a fiber orientation of 120° was tested under 0.9 W/cm² light intensity (Fig. 5g and Movie S2). The actuator transitioned from a curled to a fully extended configuration within just 12 s, exhibiting excellent response speed and shape controllability. This practical demonstration further validates the high-performance actuation capability of the CF/PLA bilayer system.

### 3.6 Light-electric coupled actuation behavior

The above analyses demonstrate that the CF/PLA bilayer actuator exhibits excellent energy conversion capabilities under single-mode stimulation. However, in practical applications, the effective light intensity received by the actuator can be significantly affected by factors such as beam

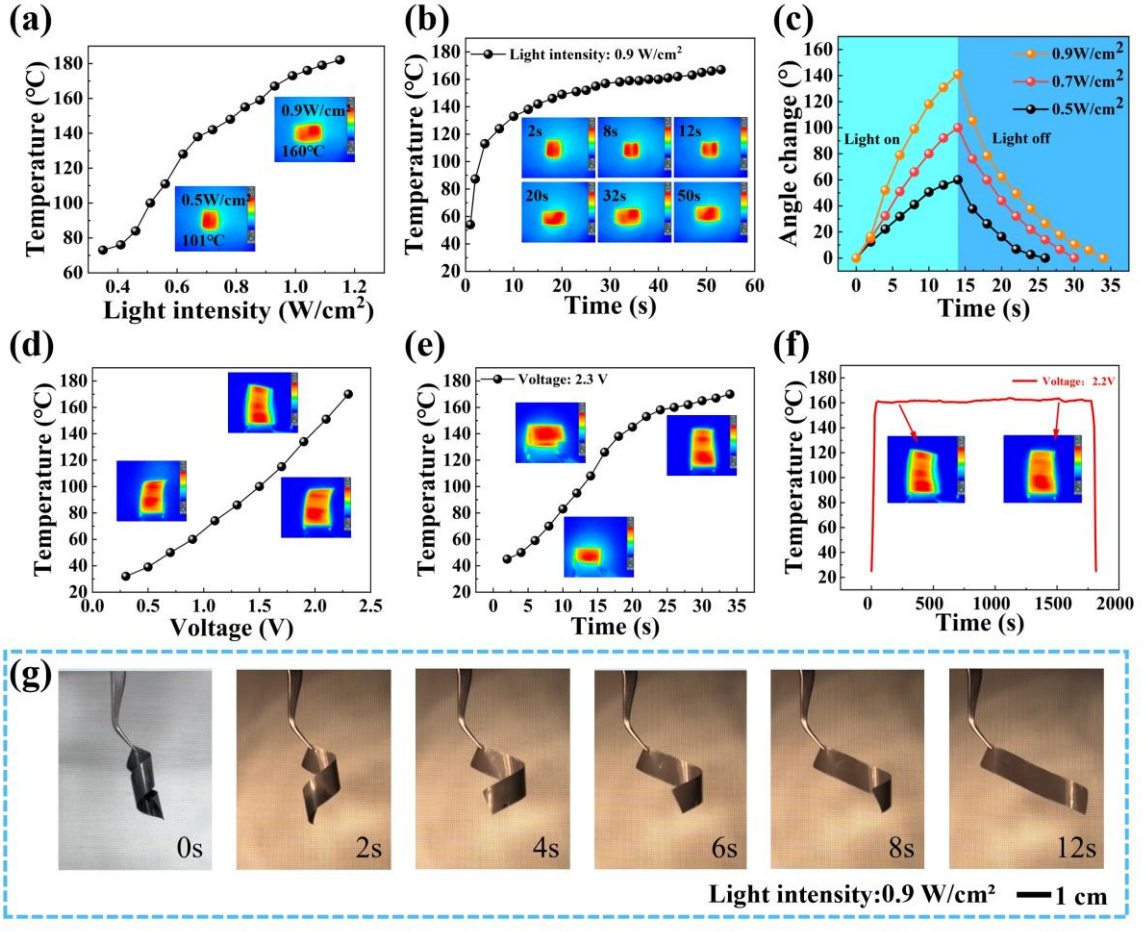


**Fig. 5:** Light and electrical stimulation response behaviors of the CF/PLA actuators: (a) Surface temperature of the CF/PLA actuator as a function of light intensity; (b) Real-time surface temperature evolution and infrared thermal images under 0.9 W/cm² illumination; (c) Actuation angle variation of the CF/PLA actuator under 0.5 W/cm², 0.7 W/cm² and 0.9 W/cm² light intensities with light on/off switching; (d) Surface temperature of the actuator as a function of applied voltage; (e) Real-time temperature evolution under a constant voltage of 2.3 V; (f) Long-term temperature stability of the actuator under continuous heating at 2.2 V; (g) Sequential snapshots of the CF/PLA actuator with a 120° fiber orientation unfolding under 0.9 W/cm² light irradiation.

size and incident angle, while electric actuation remains reliant on power supply.[22,40,43] Therefore, developing a light-electric hybrid actuation mode with flexible switching and combination potential is of great significance, particularly for scenarios requiring precise control in micro/nano systems.[12,23,27]

To investigate the mechanism of light-electric coupled actuation, we first performed systematic single-light and single-electric stimulation tests to identify 14 pairs of equivalent light intensities and voltages that induce identical bending angles (Fig. 6a). Subsequently, the deformation angle and surface temperature of the actuator were measured under both equivalent single-mode stimulation and 0.5 × strength hybrid stimulation (Figs. 6b and c). Results showed that the equilibrium angle and temperature under 0.5 × hybrid stimulation (*i.e.*, 0.5 × light intensity + 0.5 × voltage) were both lower than those under single-mode equivalent stimulation. Taking the equivalent combination of 0.78 W/cm² light intensity and 1.9 V voltage as an example, we conducted actuation tests under various light-electric ratios (Fig. 6d). It was found that the actuator's deformation amplitude under any hybrid ratio was lower than that under either single-mode condition, with the minimum deformation observed at a 5:5 ratio. Fig. 6(e) further quantifies the angle and temperature responses under different ratios of 0.78 W/cm² light and 1.9 V voltage. The results reveal that the actuation behavior is not a linear superposition of single-mode effects, but rather displays a nonlinear response.

This nonlinear behavior can be attributed to the characteristics of heat conduction, described by Fourier's law,[44] as shown in Eq. (1):

$$\Phi = -\lambda A \frac{\partial T}{\partial x} \tag{1}$$

where Φ represents the amount of heat transferred per unit time through a unit cross-sectional area A, λ is the proportionality constant, and ∂T/∂x denotes the temperature gradient in the direction normal to the interface. According to Fourier's law, the rate of heat transfer is proportional to the

temperature gradient.[45] As heat conduction increases, the rate of temperature rise slows down, leading to a reduction in thermal accumulation at dynamic equilibrium. Consequently, the final temperature under hybrid stimulation cannot reach the linear sum of single light and electric inputs.

The surface temperature variations of the CF/PLA actuator under different stimulation modes were further investigated to validate this nonlinear thermal accumulation effect (Fig. S5). The results showed that, under simultaneous light (0.67 W/cm²) and electrical (1.8 V) input, the actuator exhibited a surface temperature higher than that observed with either stimulus alone, but still significantly lower than the arithmetic sum of both. This confirmed the presence of nonlinear thermal accumulation behavior under hybrid stimuli. This observation can be further understood by analyzing the fundamental mechanism of heat transfer. When both stimuli are applied simultaneously, the internal temperature gradient $\partial T/\partial x$ increases, accelerating heat transfer and promoting faster dissipation to the surroundings. As a result, the internal temperature of the actuator under combined light and electric input is lower than the sum of temperatures generated by each individual stimulus, reflecting a nonlinear thermal response

To further verify this nonlinear enhancement effect, hybrid stimulation using 0.67 W/cm² light intensity and 1.8 V voltage was applied (Fig. 6f). The resulting bending angle exceeded that under either single stimulus alone, but remained lower than the sum of both. Notably, the actuation outcome was independent of the stimulus sequence. As shown in Fig. 6(g), whether the light and voltage were applied simultaneously, or sequentially (light followed by electric or vice versa), the actuator achieved the same maximum deformation angle (134°), despite minor differences in response time.

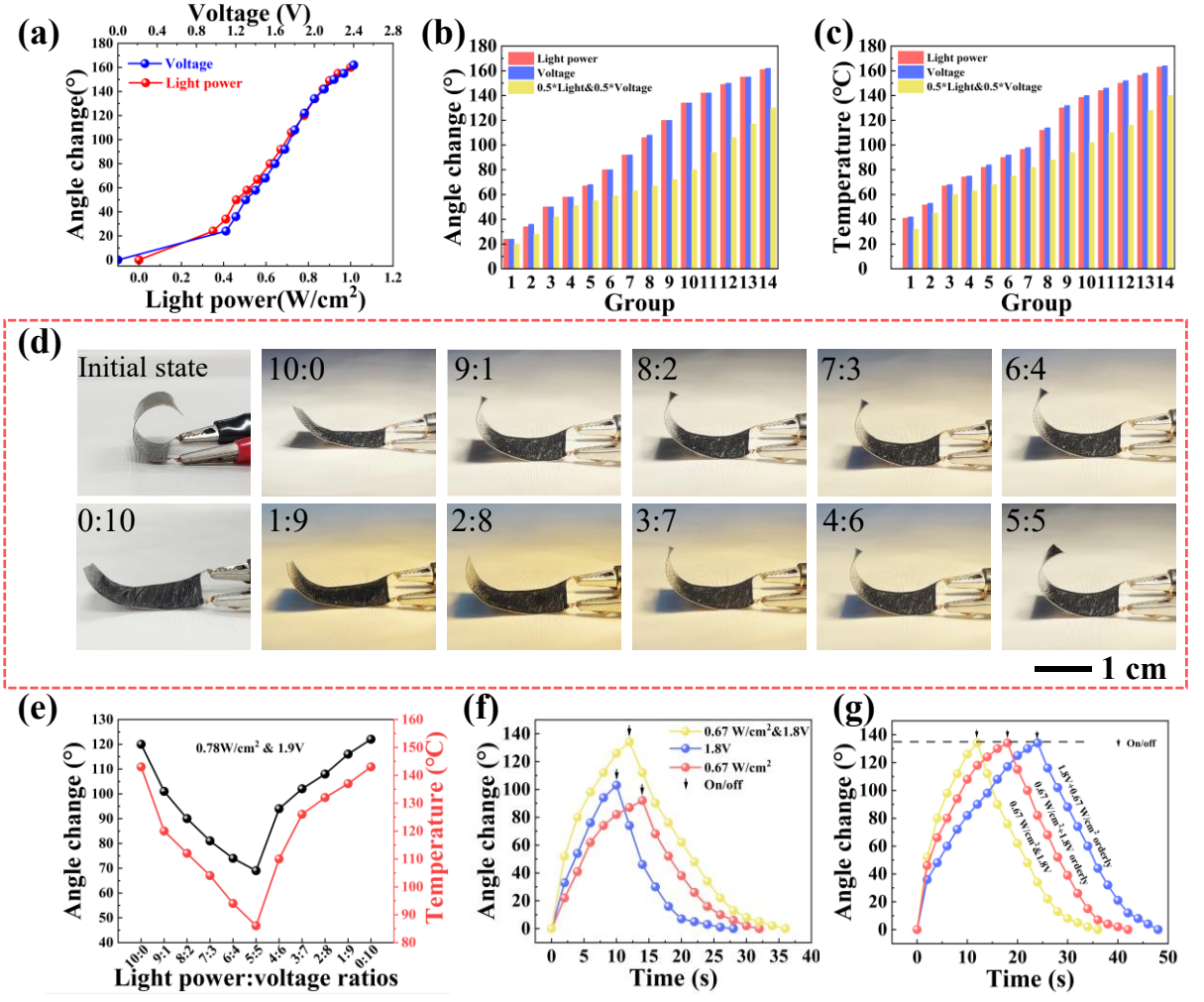


**Fig. 6:** Actuation behavior of CF/PLA actuators under light and electric synergistic response: (a) Equivalent actuation angles achieved under single visible light or electrical stimulation; (b) Actuation angles under equivalent single-mode stimulation and 0.5 × light-electric hybrid stimulation; (c) Equilibrium temperatures under equivalent single-mode stimulation and 0.5 × hybrid stimulation; (d) Photographs of actuators under hybrid stimulation at 0.78 W/cm² and 1.9 V with varying light-to-electric ratios; (e) Actuation angles and temperatures under hybrid stimulation at different light-to-electric ratios (0.78 W/cm² and 1.9 V input); (f) Time-dependent actuation angles under 0.67 W/cm² light, 1.8 V voltage, and their hybrid stimulation; (g) Angle variations under different stimulation sequences (simultaneous, light-first, and electric-first) with 0.67 W/cm² light and 1.8 V voltage.

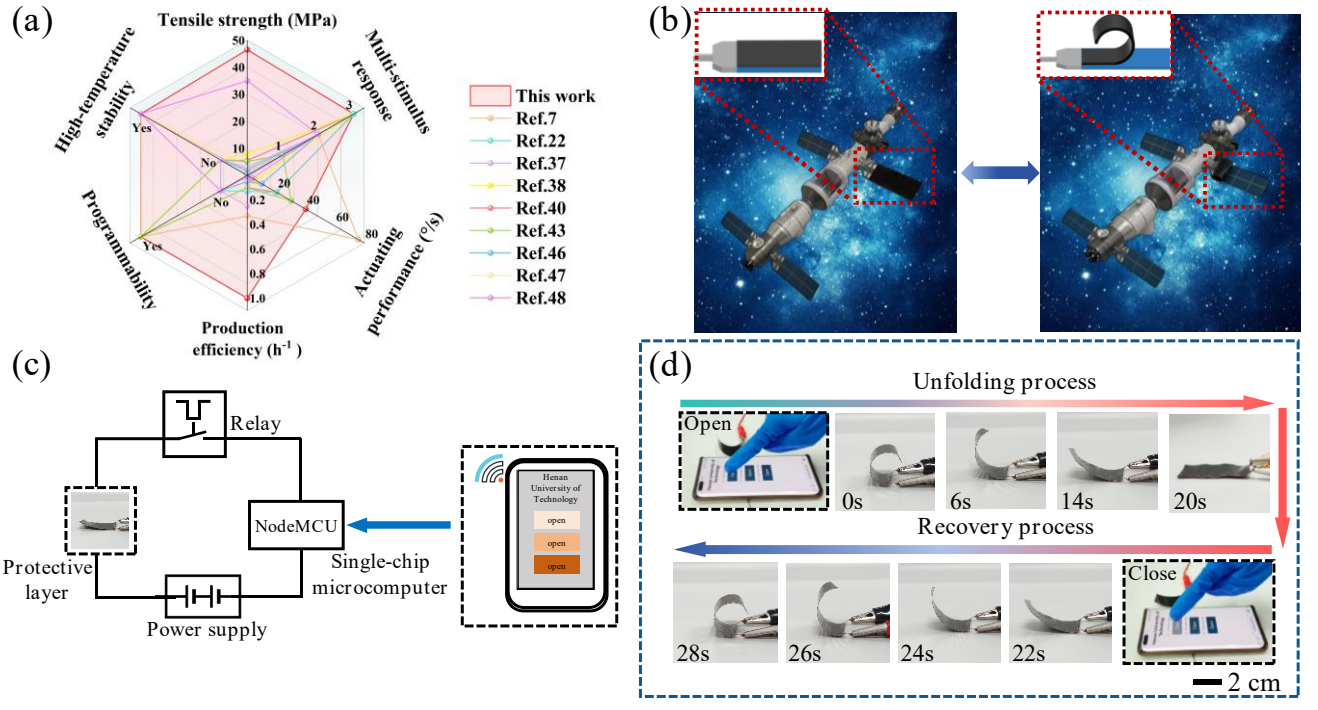


**Fig. 7:** Application of CF/PLA actuators: (a) Comparison of the overall performance of CF/PLA actuator with previously reported actuators; (b) Schematic of the controllable deployment of the space station solar sail protection layer; (c) Electrical control architecture of the CF/PLA actuator-based intelligent protection system; (d) Remote intelligent control process of the CF/PLA actuator.

### 3.7 Intelligent protection system for space environment

To evaluate the CF/PLA actuator's adaptability in complex real-world scenarios, we systematically assessed its performance across multiple dimensions. As shown in Fig. 7(a), compared to other actuators, our design exhibits significant improvements in mechanical properties, multi-stimuli responsiveness, actuation efficiency, production efficiency, programmability, and high-temperature stability.[7,22,37,38,40,43,46-48] Notably, the actuator demonstrates enhanced performance under combined light and electrical stimulation, enabling multi-field coupling and expanding its potential applications in extreme environments (Table S1).

With its excellent high-temperature tolerance and environmental robustness, the actuator was integrated into an intelligent deployment-retraction system for solar sail protection in space stations (Fig. 7b). When exposed to high-energy charged particle radiation, the actuator quickly deploys a protective layer to mitigate radiation damage.[49] As radiation intensity decreases, the actuator autonomously contracts, exposing the solar sail for continued solar energy absorption. The actuator's control system, depicted in Fig. 7(c), integrates a NodeMCU module and a DC power supply, enabling precise actuation triggered by low-voltage IoT commands. As shown in Fig. 7(d), the actuator fully deploys in 20 s and returns to its initial shape within 8 s after power is removed, demonstrating fast response and reversibility. The stable performance of this actuation system in extreme space conditions, combined with IoT control integration, offers a new path for developing deployable and retractable aerospace protection systems.

## 4. Conclusion

This study presents the development of a mechanically robust CF/PLA bilayer actuator fabricated using hot-pressing. Its heterogeneous structure, combining continuous carbon fibers and thermoplastic PLA, enables programmable deformation. Finite element analysis confirmed favorable stress distribution and thermal accumulation during actuation. Moreover, the actuator maintained stable shape recovery and high reversibility after more than 500 thermal cycles. In addition, mechanical testing revealed a high tensile strength of 1525 MPa at 0° fiber orientation, along with strong interfacial adhesion of 335 N/m between the CF and PLA layers, which validates the effectiveness of the fabrication approach. In light and electrical response tests, the actuator achieved a 160° angle change and a temperature response of 150 °C within 20 s under a light intensity of 0.9 W/cm² and 2.3 V voltage, illustrating significant deformation capability. Under combined light and electrical stimulation, the actuator exhibited a nonlinear deformation response due to thermal coupling effects. Additionally, the CF/PLA actuator enabled the design of an intelligent deployable-retractable protection system for solar sail shielding on space stations. Experimental results showed that, integrated with IoT control technology, the system could quickly deploy the protective layer under high-energy radiation and adaptively retract when radiation intensity decreased, effectively protecting the solar sail. In

summary, the CF/PLA bilayer actuator combines robust mechanical performance, strong interfacial bonding, multi-stimuli responsiveness, complex deformation, and scalability, offering a reliable solution for next-generation soft intelligent materials.

**Acknowledgments**

The authors would like to express their gratitude to Henan International Joint Laboratory of Carbon Composition Material and Henan Provincial Engineering Laboratory of Automotive Composite Materials of Henan University of Technology in China, for the funding support of the project of the National Natural Science Foundation of China, Young Scientists Fund (Grant No. 52105333), Key International Science and Technology Cooperation Project of Henan Province (Grant No. 251111520900), High Level Talent Foundation of Henan University of Technology (Grant No. 2024BS019) and the technical and facility support.

**Conflict of Interest**

There is no conflict of interest.

**Supporting Information**

Applicable.

**CRediT statement**

**Lin Jiang:** Supervision, Conceptualization, Funding Acquisition, Resources, Formal Analysis, Writing Review & Editing; **Xingyu Yue:** Methodology, Investigation, Data Curation, Writing Original Draft; **Jie Sheng:** Methodology, Investigation, Data Curation, Writing Original Draft; **Mingxia Li:** Investigation, Data Curation, Writing Original Draft; **Shengkun Jiang:** Investigation, Data Curation; **Zhengqiang Huang:** Supervision, Conceptualization, Resource; **Tie Geng:** Conceptualization, Funding Acquisition, Resources; **Haihong Wu:** Supervision, Conceptualization, Resources.

**References**

[1] X. Xu, G. Peng, B. Zhang, F. Shi, L. Gao, J. Gao, Material performance, manufacturing methods, and engineering applications in aviation of carbon fiber reinforced polymers: a comprehensive review, *Thin-Walled Structures*, 2025, **209**, 112899, doi: 10.1016/j.tws.2024.112899.

[2] H. Zhou, X. Li, C. Shao, X. Li, Y. Li, D. Li, J. Feng, X. Ding, Y. Zhu, Review on the automated fiber placement process for the aero-engine composite fan blade and its feasibility in element level, *Composites Part A: Applied Science and Manufacturing*, 2025, **193**, 108875, doi: 10.1016/j.compositesa.2025.108875.

[3] A. M. Ashteyat, A. T. Obaidat, T. F. Kharabsheh, The behavior of thermal shock repairing of high strength reinforced concrete beam using NSM-CFRP rope and strip, *Engineered Science*, 2023, **27**, 1028, doi: 10.30919/es1028.

[4] J. Xiang, H. Lin, D. Wang, Y. Rao, J. P. M. Correia, S. Ahzi, Y. Peng, K. Wang, 3D printed continuous fiber-reinforced composites with high fiber bundle shape uniformity, mechanical performance consistency, and fiber content, *Composites Communications*, 2025, **58**, 102499, doi: 10.1016/j.coco.2025.102499.

[5] Y. Hu, Y. Lin, L. Yang, S. Wu, D. Tang, C. Yan, Y. Shi, Additive manufacturing of carbon fiber-reinforced composites: a review, *Applied Composite Materials*, 2024, **31**, 353-398, doi: 10.1007/s10443-023-10178-w.

[6] Z. Tian, Y. Wang, X. Hou, Review of chemical recycling and reuse of carbon fiber reinforced epoxy resin composites, *New Carbon Materials*, 2022, **37**, 1021-1041, doi: 10.1016/S1872-5805(22)60652-8.

[7] J. Zhang, Y. Guo, W. Hu, M. Sitti, Wirelessly actuated thermo- and magneto-responsive soft bimorph materials with programmable shape-morphing, *Advanced Materials*, 2021, **33**, e2100336, doi: 10.1002/adma.202100336.

[8] H. H. Wang, S. Huo, V. Chevali, W. Hall, A. Offringa, P. Song, H. Wang, Carbon fiber reinforced thermoplastics: from materials to manufacturing and applications, *Advanced Materials*, 2025, **37**, e2418709, doi: 10.1002/adma.202418709.

[9] D. Li, J. Li, P. Wu, G. Zhao, Q.-A. Qu, X. Yu, Recent advances in electrically driven soft actuators across dimensional scales from 2D to 3D, *Advanced Intelligent Systems*, 2024, **6**, 2300070, doi: 10.1002/aisy.202300070.

[10] Y. Hao, M. Qiu, K. Dai, G. Zheng, C. Liu, C. Shen, Tendril-inspired programmable soft actuator based on bilayer thermoplastic film, *Chemical Engineering Journal*, 2025, **503**, 158524, doi: 10.1016/j.cej.2024.158524.

[11] W. Zhang, K. Jin, Z. Ren, L. Li, L. Chang, C. Zhang, R. Wang, B. Li, G. Wu, Y. Hu, High-performance MXene/carbon nanotube electrochemical actuators for biomimetic soft robotic applications, *Advanced Functional Materials*, 2024, **34**, 2408496, doi: 10.1002/adfm.202408496.

[12] M. Cheng, Q. Li, Left-handed or right-handed? determinants of the chirality of helically deformable soft actuators, *Soft Robotics*, 2022, **9**, 850-860, doi: 10.1089/soro.2021.0067.

[13] W. Li, C. Lou, S. Liu, Q. Ma, G. Liao, K. C. Leung, X. Gong, H. Ma, S. Xuan, Climbing plant-inspired multi-responsive biomimetic actuator with transitioning complex surfaces, *Advanced Functional Materials*, 2025, **35**, 2414733, doi: 10.1002/adfm.202414733.

[14] W. Li, M. Sang, S. Liu, B. Wang, X. Cao, G. Liu, X. Gong, L. Hao, S. Xuan, Dual-mode biomimetic soft actuator with electrothermal and magneto-responsive performance,

*Composites Part B*: *Engineering*, 2022, **238**, 109880, doi: 10.1016/j.compositesb.2022.109880.

[15] R. Ruiz-Iglesias, R. Cappello, O. T. Thomsen, J. M. Dulieu-Barton, Estimating the coefficients of thermal expansion of carbon fibre composite materials using infrared thermography, *Composites Part A*: *Applied Science and Manufacturing*, 2025, **198**, 109094, doi: 10.1016/j.compositesa.2025.109094.

[16] F. Richter, D. Wu, Interfacial adhesion between dissimilar thermoplastics fabricated *via* material extrusion-based multi-material additive manufacturing, *Materials & Design*, 2025, **252**, 113688, doi: 10.1016/j.matdes.2025.113688.

[17] H. Xu, H. Zhan, Z. Xu, C. Jing, Q. Chen, M. Zhu, L. Kong, X. Fan, Y. Qing, S. Wen, C. Wang, F. Luo, Sandwich-like CNTs/Carbon@$Si_3N_4$ porous foam for temperature-insensitive electromagnetic wave absorption, *Advanced Functional Materials*, 2025, **35**, 2421242, doi: 10.1002/adfm.202421242.

[18] Y. Hao, W. Yao, C. Shi, G. Liang, A. She, Electrothermal stability and durability evaluation of CFRC optimized with CB/$Fe_3O_4$ under complex environmental conditions: an experimental study, *Construction and Building Materials*, 2025, **458**, 139567, doi: 10.1016/j.conbuildmat.2024.139567.

[19] Z. Li, Z. Teng, W. Yang, W. Wang, C. Zhang, S. Li, 2D patterning and 3D hierarchical recovery of waste carbon fiber reinforced polymers *via* programmable laser strategy, *Fuel*, 2025, **390**, 134687, doi: 10.1016/j.fuel.2025.134687.

[20] S. D. Amer, M. Assad, R. A. Hawileh, G. Karak, H. Safieh, J. Abdalla, Prediction of ultimate strain in anchored CFRP laminates using machine learning, *Engineered Science*, 2024, **31**, 1251, doi: 10.30919/es1251.

[21] Y. Chen, C. Valenzuela, X. Zhang, X. Yang, L. Wang, W. Feng, Light-driven dandelion-inspired microfliers, *Nature Communications*, 2023, **14**, 3036, doi: 10.1038/s41467-023-38792-z.

[22] L. Liu, Y. Li, Z. Lu, R. Miao, N. Zhang, Thermal and light-driven soft actuators based on a conductive polypyrrole nanofibers integrated poly(N-isopropylacrylamide) hydrogel with intelligent response, *Journal of Colloid and Interface Science*, 2024, **675**, 336-346, doi: 10.1016/j.jcis.2024.07.017.

[23] L. Chang, D. Wang, Z. Huang, C. Wang, J. Torop, B. Li, Y. Wang, Y. Hu, A. Aabloo, A versatile ionomer-based soft actuator with multi-stimulus responses, self-sustainable locomotion, and photoelectric conversion, *Advanced Functional Materials*, 2023, **33**, 2212341, doi: 10.1002/adfm.202212341.

[24] Wang L, Sun X, Wang D, An integrated, multi-functional intrinsic responsive foldable protective layer for space station solar panels, *Energy*, 2024, **303**, 131825, doi: 10.1016/j.energy.2024.131825.

[25] L. Wang, X. Sun, D. Wang, P. Cui, J. Wang, Q. Li, High-precision, programmable soft wireless robotics for cooling tower cleaning based on Internet of Things technology, *Chemical Engineering Journal*, 2024, **495**, 153268, doi: 10.1016/j.cej.2024.153268.

[26] Y. Dong, L. Wang, N. Xia, Y. Wang, S. Wang, Z. Yang, D. Jin, X. Du, E. Yu, C. Pan, B.-F. Liu, L. Zhang, Multi-stimuli-response programmable soft actuators with site-specific and anisotropic deformation behavior, *Nano Energy*, 2021, **88**, 106254, doi: 10.1016/j.nanoen.2021.106254.

[27] H. Li, Z. Wu, Y. Xing, B. Li, L. Liu, Photoelectric synergistic response properties of the $Ti_3C_2T_x$ MXene-CNT/PDMS bilayer actuator, *Nano Energy*, 2022, **103**, 107821, doi: 10.1016/j.nanoen.2022.107821.

[28] H. Li, Y. Liang, G. Gao, S. Wei, Y. Jian, X. Le, W. Lu, Q. Liu, J. Zhang, T. Chen, Asymmetric bilayer CNTs-elastomer/hydrogel composite as soft actuators with sensing performance, *Chemical Engineering Journal*, 2021, **415**, 128988, doi: 10.1016/j.cej.2021.128988.

[29] J. Zuo, H. Chen, J. Gu, W. Zhang, Z. Zhang, G. Huang, A facile method for fabricating humidity-sensitive bilayer actuators with programmable deformation, *Sensors and Actuators A*: *Physical*, 2023, **352**, 114208, doi: 10.1016/j.sna.2023.114208.

[30] Y. Zhang, S. Xie, D. Zhang, B. Ren, Y. Liu, L. Tang, Q. Chen, J. Yang, J. Wu, J. Tang, J. Zheng, Thermo-responsive and shape-adaptive hydrogel actuators from fundamentals to applications, *Engineered Science*, 2019, **6**, 1-11, doi: 10.30919/es8d788.

[31] M. Mulle, R. Zitoune, F. Collombet, P. Olivier, Y. H. Grunevald, Thermal expansion of carbon–epoxy laminates measured with embedded FBGS–Comparison with other experimental techniques and numerical simulation, *Composites Part A*: *Applied Science and Manufacturing*, 2007, **38**, 1414-1424, doi: 10.1016/j.compositesa.2006.08.008.

[32] C. Hu, Y. Zhang, X. Pang, X. Chen, Poly(lactic acid): recent stereochemical advances and new materials engineering, *Advanced Materials*, 2025, **37**, 2412185, doi: 10.1002/adma.202412185.

[33] L. Liu, Y. Wang, C. Cheng, S. Lyu, Z. Zhu, Preparation of phosphorus-doped chitosan derivative and its applications in polylactic acid: Crystallization, flame retardancy, anti-dripping and mechanical properties, *International Journal of Biological Macromolecules*, 2024, **265**, 130648, doi: 10.1016/j.ijbiomac.2024.130648.

[34] J. Ge, G. Catalanotti, B. G. Falzon, C. Higgins, C. McClory, J. A. Thiebot, L. Zhang, M. He, Y. Jin, D. Sun, Process characteristics, damage mechanisms and challenges in machining of fibre reinforced thermoplastic polymer (FRTP) composites: a review, *Composites Part B*: *Engineering*, 2024, **273**, 111247, doi: 10.1016/j.compositesb.2024.111247.

[35] M. S. Barkhad, B. Abu-Jdayil, A. H. I. Mourad, M. Z. Iqbal, Thermal insulation and mechanical properties of polylactic acid

(PLA) at different processing conditions, *Polymers*, 2020, **12**, 2091, doi: 10.3390/polym12092091.

[36] S. Li, H. Yang, G. Chen, J. Zheng, W. Wang, J. Ren, C. Zhu, Y. Yang, Y. Cong, J. Fu, 4D printing of biomimetic anisotropic self-sensing hydrogel actuators, *Chemical Engineering Journal*, 2023, **473**, 145444, doi: 10.1016/j.cej.2023.145444.

[37] S. Mun, S. Lee, K. J. Bae, Y. Bae, H.-M. Lee, B.-J. Kim, J. Yu, S. Park, Bio-imitative synergistic color-changing and shape-morphing elastic fibers with a liquid metal core, *Advanced Fiber Materials*, 2024, **6**, 900-910, doi: 10.1007/s42765-024-00399-4.

[38] S. Ma, P. Xue, C. Valenzuela, X. Zhang, Y. Chen, Y. Liu, L. Yang, X. Xu, L. Wang, Highly stretchable and conductive MXene-encapsulated liquid metal hydrogels for bioinspired self-sensing soft actuators, *Advanced Functional Materials*, 2024, **34**, 2309899, doi: 10.1002/adfm.202309899.

[39] F. Puza, K. Lienkamp, 3D printing of polymer hydrogels: from basic techniques to programmable actuation, *Advanced Functional Materials*, 2022, **32**, 2205345, doi: 10.1002/adfm.202205345.

[40] Y. Zhang, X. Zhou, L. Liu, S. Wang, Y. Zhang, M. Wu, Z. Lu, Z. Ming, J. Tao, J. Xiong, Highly-aligned all-fiber actuator with asymmetric photothermal-humidity response and autonomous perceptivity, *Advanced Materials*, 2024, **36**, e2404696, doi: 10.1002/adma.202404696.

[41] R. M. Erb, J. S. Sander, R. Grisch, A. R. Studart, Self-shaping composites with programmable bioinspired microstructures, *Nature Communications*, 2013, **4**, 1712, doi: 10.1038/ncomms2666.

[42] J. Heremans, I. Rahim, M. S. Dresselhaus, Thermal conductivity and Raman spectra of carbon fibers, *Physical Review B*, 1985, **32**, 6742-6747, doi: 10.1103/physrevb.32.6742.

[43] X. Wei, Y. Xue, Y. Sun, L. Chen, C. Zhang, Q. Wu, S. Peng, C. Ma, Z. Liu, S. Jiang, X. Yang, S. Agarwal, G. Duan, A robust anisotropic light-responsive hydrogel for ultrafast and complex biomimetic actuation *via* poly(pyrrole)-coated electrospun nanofiber, *Chemical Engineering Journal*, 2023, **452**, 139373, doi: 10.1016/j.cej.2022.139373.

[44] T. N. Narasimhan, Fourier's heat conduction equation: History, influence, and connections, *Proceedings of the Indian Academy of Sciences - Earth and Planetary Sciences*, 1999, **108**, 117-148, doi: 10.1007/BF02842327.

[45] X. Xu, J. Chen, J. Zhou, B. Li, Thermal conductivity of polymers and their nanocomposites, *Advanced Materials*, 2018, **30**, 1705544, doi: 10.1002/adma.201705544.

[46] W. Ai, J. Wu, Y. Long, K. Song, A rolling light-driven pneumatic soft actuator based on liquid-gas phase change, *Advanced Materials*, 2025, **37**, e2418218, doi: 10.1002/adma.202418218.

[47] X. Shi, K. Zhang, J. Chen, H. Qian, Y. Huang, B. Jiang, Octopi tentacles-inspired architecture enables self-healing conductive rapid-photo-responsive materials for soft multifunctional actuators, *Advanced Functional Materials*, 2024, **34**, 2311567, doi: 10.1002/adfm.202311567.

[48] Z. Huang, Z. Wu, C. Li, X. Li, X. Yang, X. Qiu, Y. Wang, Y. Miao, X. Zhang, Self-healing yet strong actuator materials with muscle-like diastole and contraction *via* multilevel relaxations, *Advanced Materials*, 2025, **37**, 2413194, doi: 10.1002/adma.202413194.

[49] E. F. Sukur, Thermally conditioned aerospace-grade carbon fiber reinforced polyether ketone ketone composites: Structure, impact response, and thermomechanical performance, *Polymer Composites*, 2023, **44**, 2530-2544, doi: 10.1002/pc.27261.